Available online at www.eccomasproceedia.org
Eccomas Proceedia COMPDYN (2025) 2012-2023

ECCOMAS
Proceedia

COMPDYN 2025
10th ECCOMAS Thematic Conference on
Computational Methods in Structural Dynamics and Earthquake Engineering
M. Papadrakakis, M. Fragiadakis (eds.)
Rhodes Island, Greece, 15-18 June 2025

DEFORMABILITY OF STEEL-CONCRETE COMPOSITE SLABS

M. Simoncelli

Politecnico di Milano
Department of Architecture, Built environment and Construction engineering
Piazza Leonardo da Vinci 32, 20133 Milano
marco.simoncelli@polimi.it

Abstract

Steel-concrete composite slabs provide an excellent flooring solution, leveraging the key properties of two materials: steel, used for the decking, and concrete, which may be reinforced or not. Due to the impossibility of ensuring full interaction between the two materials, the design is primarily governed by horizontal shear-bond strength, which must be experimentally assessed. While the procedure for evaluating actual resistance has been extensively studied and is now well-established, further investigations are still required for the estimation of flexural stiffness.
At the serviceability limit state (SLS), slab deformability -and consequently, also the vibration modes- are critical factors influencing the overall design. In this context, this paper presents a discussion about the deformability of steel-concrete composite slabs. Specifically, based on experimental tests on slabs of varying lengths (2000, 2400, 2800, 3200, and 3600 mm), under monotonic and cyclic loads, the influence of cracking on the flexural response is discussed. Finally, a numerical finite element strategy is briefly presented to capture their structural response.

Keywords: Composite concrete-steel slab, Recycled aggregates, Global deformability, finite element numerical models.

Peer-review under responsibility of the organizing committee of COMPDYN 2025.
doi: 10.7712/120125.12547.24499

1 INTRODUCTION

Steel–concrete composite slabs, similar to composite beams and columns, offer a highly effective structural solution by efficiently utilizing the properties of both materials: steel and concrete. In flexural applications, concrete primarily resists compressive stresses, while tensile forces are absorbed by the steel within the hi-bond corrugated sheet, which also serves as a temporary working platform for wet concrete during construction [1, 2].

Typically, these slabs are constructed without additional reinforcement bars within the steel ribs, having only a welded steel wire mesh placed at the top to control shrinkage and mitigate the effects of transverse tensile stresses caused by localized vertical loads. The market generally offers two main types of hi-bond steel sheeting: in the United States, re-entrant profiles (Figure 1a) are the most prevalent, whereas in Europe, trapezoidal metal decking (Figure 1b) is more commonly used. Notably, in certain countries such as Italy, only trapezoidal decks are manufactured and available, as their relatively low production cost is offset by the high expense of transportation.

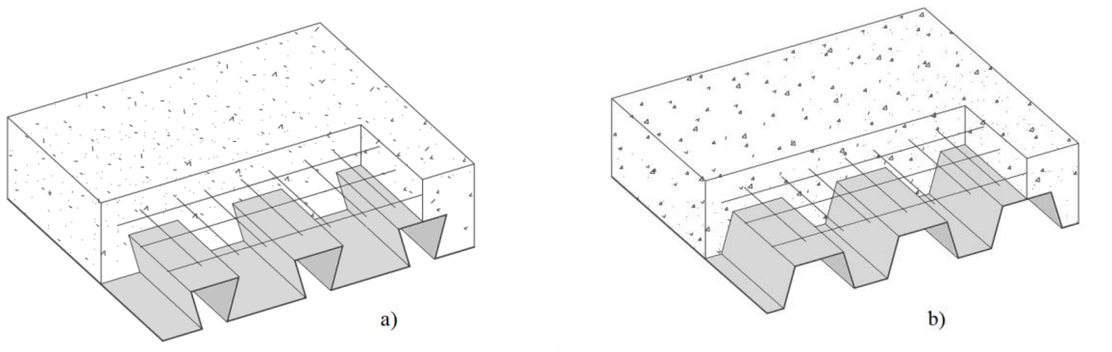

Figure 1: Typical steel-concrete slab with different hi-bond typology [3].

The composite slab performances, in terms of strength, stiffness and ductility, mainly depend on the transfer of longitudinal shear stresses between the concrete slab and the profiled sheet. The steel ribs are filled with concrete and the steel-concrete contact surface transfers the longitudinal shear between the two materials, guaranteeing the composite action. Longitudinal shear is then transferred by the mechanical interlocks, protrusions, indentations and embossments produced in the profile during the working process.

The ultimate resistance of composite slabs has been greatly studied over the years [4,5], producing several design rules contained in the main worldwide codes [6,7]. Longitudinal shear failure mode governs generally the load carrying capacity can be estimated using either the shear-bond (also identified as m-k) or the partially shear connection (PSC) methods [7]. Moreover, both strategies assume that at the ultimate limit state, the steel sheet response is always in the plastic range independently on the effective strain value reached at the various levels of the cross-section. Furthermore, the contribution of the concrete inside the ribs is always neglected. These simplified assumptions affect the resistance domain and could lead to a non-reliable estimation of the level of interaction between concrete and steel. As observed by different researchers [3, 8] once a limit strain ε_{lim} of the lower edge of the steel deck is reached (evaluated as total strain minus the one existing before bond of concrete, due to the dead weight) longitudinal shear collapse occurs, with a large part of the steel deck in the elastic range. This aspect emphasizes that the hypothesis of a spread plasticity along the steel cross-section cannot be considered as realistic. In the Eurocode [7], a main distinction between fragile and ductile behavior is reported classifying as a ductile response the slabs which showed an increasing load after the initial debonding.

For what concerns the global deformability, in [9, 10] several composite slabs have been experimentally tested, with different length and concrete type. It has been shown that the slab response can be divided into two separate stages: the initial stage where the two materials are perfectly coupled, and a second part after the debonding. However, no discussion about the cracking in the concrete is made. Concrete cracking is one of the most principal causes of the increasing of the slab deformability. As discussed in Eurocode 4, the deformability of a slab can be evaluated considering an average stiffness between cracked and un-cracked concrete.

To investigate this assumption, in the current paper, the deformability of different slabs having the same metal sheeting, but different global lengths have been evaluated. Five different lengths (2000, 2400, 2800, 3200 and 3600 mm) were considered and for each length two specimens were tested. Experimental tests were performed in accordance with EN1994-1-1 considering a four-point bending beam. The slabs deformability is discussed focusing attention on the influence of cracks into the global response. Finally, an advanced Finite Element model, developed inside ABAQUS [11] software, is proposed and discussed.

2 SUMMARY OF THE EXPERIMENTAL ACTIVITY

2.1 Test setup

The experimental configuration was established following the guidelines of EN 1994-1-1. As illustrated in Figure 2, the structural response was assessed through four-point bending tests, where concentrated loads were applied at quarter-span intervals between the two vertical supports. To maintain uniform boundary conditions, the distance from the support centerlines to the specimen edges remained below 100 mm, averaging 80 mm.

Displacement-control load was implemented, enabling continuous monitoring of key deformation parameters. Linear variable transducers (LVDTs) were employed to measure displacements at both ends of the mid-span cross-section, as well as the relative slip between the steel and concrete layers. In particular, two sensors (d2 and d3) were positioned at mid-span, while four additional transducers (d4, d5, d6, and d7) monitored lateral displacements.

The concrete was cast *on-site* within a controlled laboratory environment, ensuring stable humidity and temperature conditions throughout the curing process to enhance material consistency and test reliability.

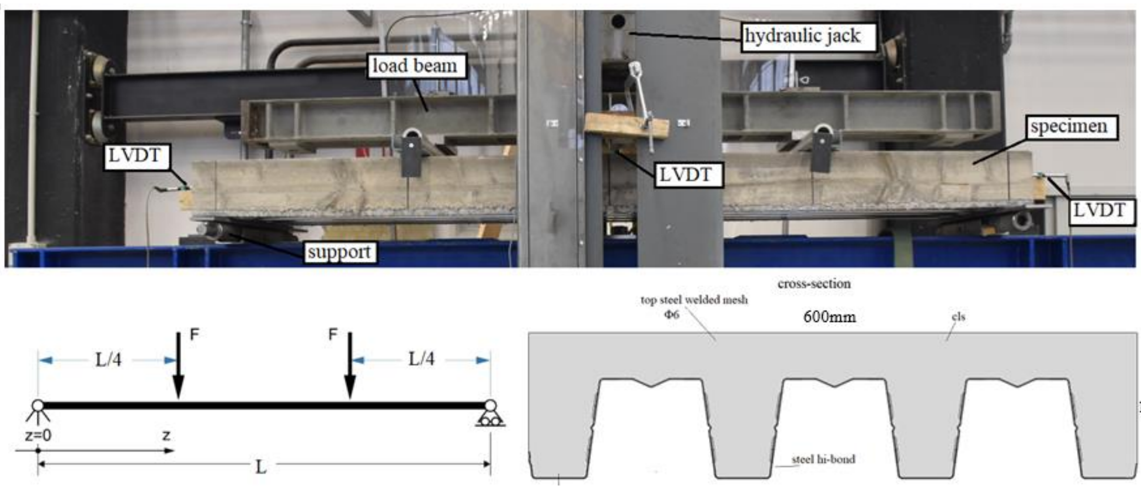

Figure 2: Test setup in accordance with EN1994-1-1 [7].

The EC4 load protocol was followed, and in particular, for each couple of nominally equal specimens:

- first specimen was loaded with an increasing monotonic load until the collapse. This test is identified with the letter M, i.e. monotonic. The ultimate load, F_{max}, was assumed as the force for which the slip between steel and concrete started;
- second specimen was tested under a cyclic load which ranged from 0.2 to 0.6 the previous ultimate load. This test is identified with the letter C, i.e. cyclic. More than 5000 cycles were applied in a period not less than 3 hours (nominally 3.5 hours). Once the cyclic load protocol was finished the load was monotonically increased until the slippage.

In all the tests, the collapse was characterized by loss of adherence at the interface between the two materials, leading to the loss of the composite actions, and consequently to typical cracks associated with the poor tensile resistance of the concrete.

2.2 Materials characteristics

The steel was nominally a S280GD grade with a constant thickness of 0.78mm. Tensile characteristics have been experimentally evaluated on three nominally equal coupons extracted from the virgin material of the coil: the mean yielding value was equal to f_y = 338 MPa while the averaged ultimate value, f_u, was 593 MPa with a Young modulus E_s equal to 195 GPa. The metal sheeting was characterized by a trapezoidal cross-section with a height of 110 mm and a width of 600 mm. Total slabs height was 180mm.

The concrete was a Portland limestone cement type II with chemical requirements (Sulphates (as SO3) $\leqslant$ 4.0%, Chloride $\leqslant$ 0.10%). Aggregates were characterized by a maximum diameter of 5.0 and 12.5 mm for the fine and the coarse ones, respectively. Potable water, without any additives, was used in the production of the mix designs (water-cement ratio equal to 0.51. The average compression resistance of the concrete obtained on five cubic samples, f_c, at 28 days of aging, is equal to 32 MPa.

2.3 Test results

Typical results obtained from the tests are reported, as an example, in Figures 3a and 3b, representing the force-middle displacement and the force-lateral displacement graphs, respectively, for the slab with 2000mm of length.

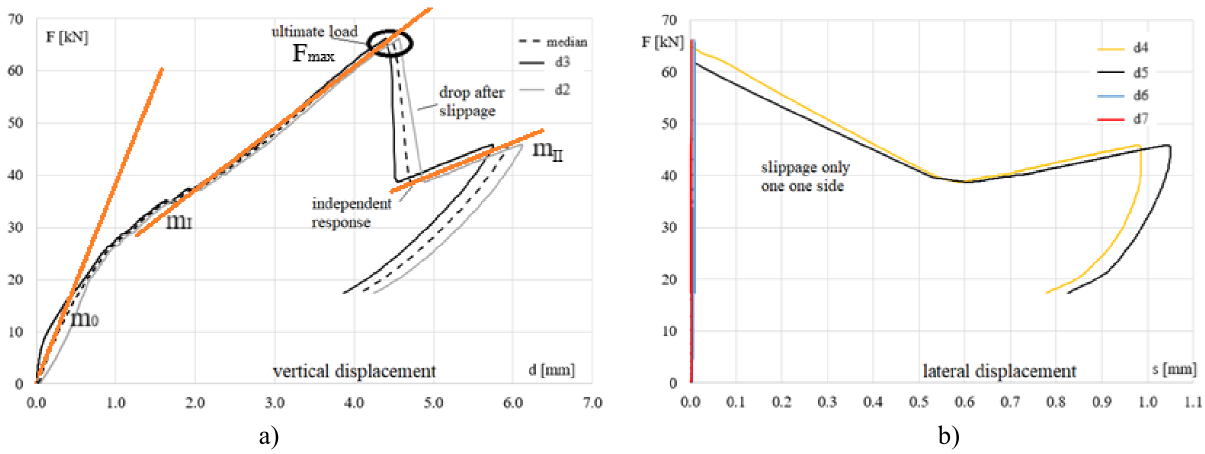

Figure 3: Typical force-displacement response: (a) d2, d3 channels and (b) d4-d7 channels, 2000mm length slab.

The first linear phase, which is characterized by the initial slab stiffness, was identified by the slope m_0. Subsequently, due to the extension of the concrete cracking it can be identified a variation of the slope in the curve, until the reaching of the full debonding load, F_{max}. This second slope can be identified with m_I. Upon reaching the maximum load, the whole debonding initiates (Figure 4), resulting in a sudden decline in the curve. This initial debonding phase is succeeded by a flexural mechanism, inducing substantial deformations despite minimal load variation. With the progression of cracking, the bond between the concrete and the steel further deteriorates, facilitating the expansion of the debonded region, until the concrete and the steel are acting as two separate materials. The slope of this last part can be identified as m_{II}. The severity of debonding and the capacity of the remaining bonded areas determine whether the composite slab experiences flexural failure in localized regions, at the ultimate load, Fu. This failure mode can manifest through cracking, excessive deflection, or in extreme scenarios, complete collapse.

(a) (b)

Figure 4: (a) Debonding at F_{max} and (b) flexural cracking of the concrete at the end of the tests.

A similar behavior characterizes the response of the slabs in the II phase of the tests. As an example, Figure 5 the response can be considered where the same 2000 mm slab is reported.

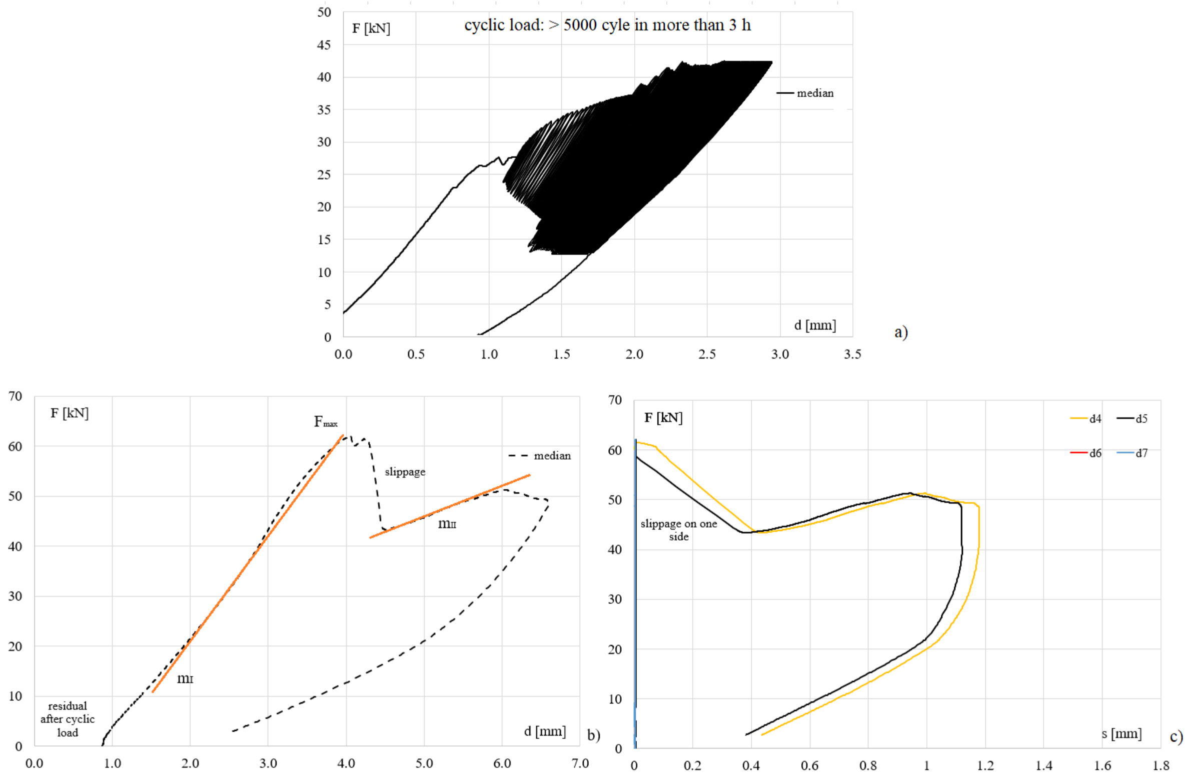

Figure 5: Typical force-displacement response after cyclic load protocol: (a) cyclic load, (b) d2, d3 channels and (c) d4-d7 channels, 2000mm length slab.

In particular, Figure 5a represents the force -vertical displacement response during the cyclic phase, while Figures 5b and 5c depict the force displacement after the cyclic phase until the collapse. If the monotonic curve is observed (Figure 5b), it can be noted that for these cases the flexural stiffness which characterizes the response, m_I, remains constant until the debonding. In fact, the slab is already cracked, after the cyclic load, and the stiffness previously identified as m_0 is not present. After the debonding the same m_{II} stiffness is observed.

The ultimate loads obtained from the tests are reported in Table 1; are reported. The experimental results for all the tested slabs are compared in terms of stiffness m_0, m_I, m_{II} in Table 1, considering both monotonic (M-test) and cyclic (C-test) load scenarios. Moreover, in the same table, the debonding load, F_{max}, is reported too.

Table 1: Principal experimental results, for all the tested slabs.

length [mm]	type of test	F_{max} [kN]	m_0 [kN/mm]	m_I [kN/mm]	m_{II} [kN/mm]
2000	M	44.3	31.98	12.10	6.20
	C	41.0	-	15.50	4.50
2400	M	42.6	16.51	7.48	3.13
	C	45.2	-	9.51	3.20
2800	M	50.4	16.08	4.72	1.29
	C	69.9	-	5.51	1.10
3200	M	58.6	14.66	3.71	0.98
	C	61.7	-	3.98	0.80
3600	M	66.2	11.57	2.38	0.85
	C	62.6	-	3.10	0.84

It can be noted that the m_I stiffness is always greater when evaluated on the specimen after the Cyclic tests. On the other hand, the final m_{II} stiffness which is evaluated after the slippage, when the two material works completely independently, is not depending on the test type.

3 GLOBAL FLEXURAL STIFFNESS OF THE SLABS

To estimate the deformability, European standards recommend adopting the average between the cracked and the uncracked moment of inertia of the entire composite cross-section [9]. To validate this approach, cracked and uncracked cross-section are evaluated. The composite slab is considered as an equivalent reinforced concrete T-shape cross-section, with the profiled steel sheeting acting as a reinforcement bar at its plastic centroid (Figure 6).

The uncracked second moment of area, considering the complete interaction between the two materials, according to the dimensions presented in Figure 6, is hence equal to:

$$I_u = \frac{1}{n}\left[\frac{bh_c^3}{12} + bh_c\left(y_T - \frac{h_c}{2}\right)^2 + \frac{b_c h_p^3}{12} + b_c h_p\left(h - y_T - \frac{h_p}{2}\right)^2\right] + I_p + A_p\left(d_p - y_T\right)^2 \quad (1)$$

where n is the homogenization factor equal to E_s/E_c. The position of the neutral axis is:

$$y_T = \frac{\frac{bh_c^2}{2} + (b_c h_p)\left(h_c + \frac{h_p}{2}\right) + nA_p d_p}{bh_c + b_c h_p + nA_p} \quad (2)$$

When the tensile tension is overpassed, cracks appear on the concrete section bringing to a new position of the neutral axis, which can be evaluated by solving a second order equilibrium equation:

$$y_{cr} = \frac{nA_p}{b}\left(-1 + \sqrt{1 + \frac{2b\,d_p}{n\,A_p}}\right) \tag{3}$$

The cracked second moment of area, neglecting the presence of concrete below the neutral axis, is:

$$I_{cr} = \frac{b y_{cr}^3}{3\,n} + I_p + A_p(d_p - y_{cr})^2 \tag{4}$$

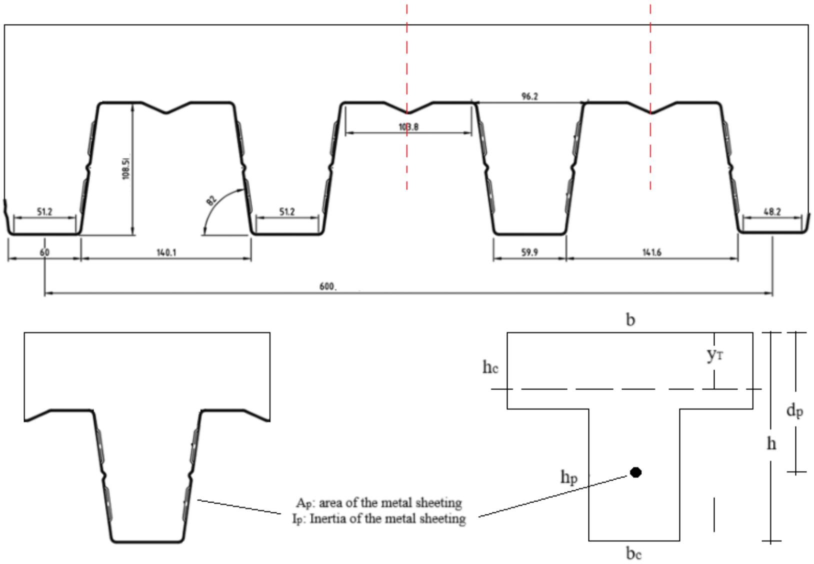

Figure 6: Equivalent T-section for the composite slab considered.

In Figure 7 the experimental flexural stiffness obtained from the monotonic tests (M-tests), are compared with theoretical ones. The theoretical results are proposed considering short-term response of the concrete, i.e. *n* is approximately equal to 6. To compare the results, the terms E_sI_u and E_sI_{cr} were considered. From Table 1, the experimental flexural stiffness is evaluated as:

$$E_s I_i = \frac{11}{768} m_i L^3 \tag{5}$$

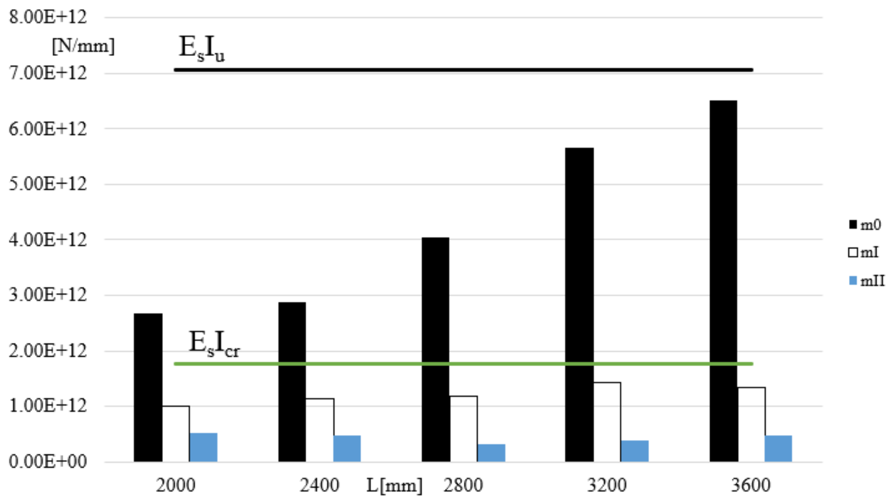

Figure 7: Flexural stiffness for all the tested slabs, M-tests.

It can be noted that, in this condition, the initial flexural stiffness of the slabs, represented by m_0, is always between the one of the cracked and uncracked cross-sections. It is interesting to notice that contrary to what one might expect at a theoretical level, the slab stiffness depends on its total length. This phenomenon can be explained by the different distribution of cracked and uncracked sections along the length of the whole slab. In fact, considering the casting process and the handling of the slabs before testing, it can be assumed that slabs with a shorter span experienced more extensive cracking diffusion compared to those with a longer span. Moreover, the flexural stiffness in the second part of the curve or after the cyclic load, represented by m_I, is always lower than the one associated with the cracked cross-section. This can be explained by the existence of a partial interaction between the two materials before the final debonding load. In fact, it seems that the concrete-steel slabs start as a monolithic section with cracks along their length and, with the increasing of the load, the cracks spread along the whole slab and a partial interaction response takes place.

Moreover, in Figure 8, the theoretical long-term response, i.e. *n* equal to almost 18, can be observed compared to the results obtained after the cyclic load (C-tests).

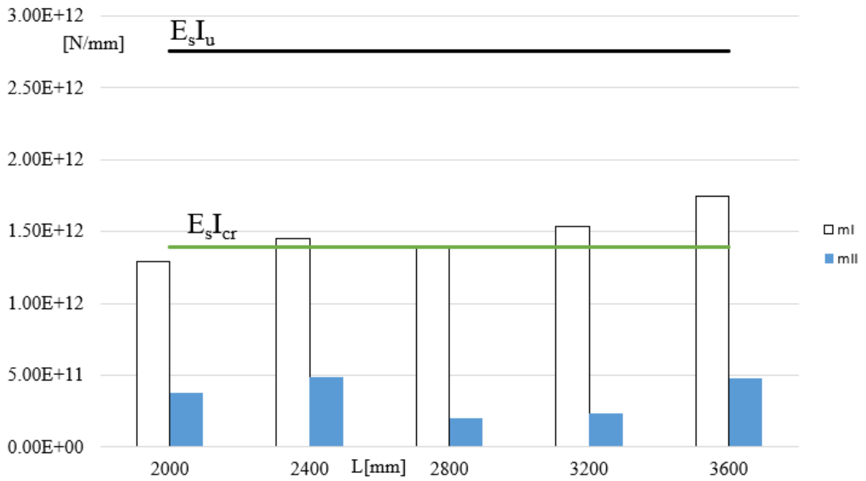

Figure 8: Flexural stiffness for all the tested slabs, C-tests.

For these cases the stiffness of the slabs can be correctly captured by considering long-term fully cracked response. The post slippage response is comparable to the previous ones obtained from the M-tests.

It should be concluded that while for the short-term response the median value between cracked and un-cracked concrete can be representative of the slab response, when the long-term response is considered, only the cracked response is acceptable.

4 PROPOSED NUMERICAL MODEL

To investigate the flexural response also via numerical models, finite element (FE) models were developed by means of the use of the commercial ABAQUS software [11]. Two parts (steel sheeting and the concrete layer) were generated and assembled inside the assembly module. The concrete was modelled with 8-node hexahedral *solid* element (CD8R) while the 4-node quadrilateral *shell* elements (S4R) were implemented for the steel deck (Figure 9). The size of the FE mesh was calibrated to optimize analysis time without compromising result accuracy. The reinforced bars on the top of the slabs were not modelled since they were used only for the shrinkage and do not contribute to the global structural response. Simply supported boundary conditions and a prescribed incremental transverse displacement, used for displacement control simulation, were applied to simulate the four-point loading scheme adopted in the tests. The loading was defined by specifying a Reference Point (RP) and assigning a prescribed dis-placement to the RP. The RP position was aligned by the center line of the composite slab span length. The explicit dynamic solver was used to perform a non-linear incremental analysis in dis-placement control.

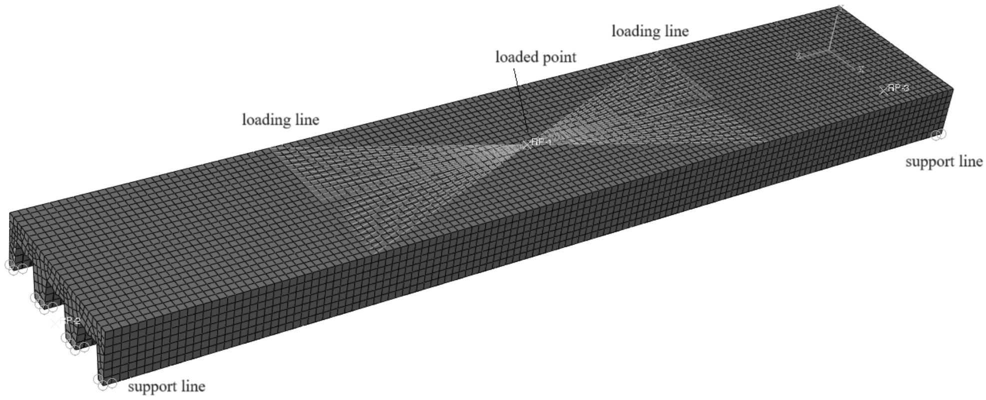

Figure 9: Finite element Numerical model of the slab.

The steel was modeled as elastic-plastic, considering true stress and logarithmic strain, derived from the tensile test results on the dog-bone specimens extracted from the metal sheeting. For the plasticity, Von-Mises yield surface criterion was utilized, considering an isotropic hardening model. For the concrete, the Concrete Damage Plasticity (CDP) was used. Two different concrete failure mechanisms were considered: compressive crushing and tensile cracking. The concrete response in compression is modeled as an initial linear response, characterized by its elastic modulus, followed by a plastic response, beyond the compression strength, and by a softening branch. Compressive concrete stress is a function of the strain followed by inelastic behavior. The response of concrete in tension is more challenging; in this paper a linear strain-softening model is adopted.

The calibration of material interaction is of paramount importance. Once defined the value of the longitudinal shear strength, different strategies can be adopted inside the software. The first step is always to assign to the whole slab the *hard contact property* to avoid compenetrating of the surfaces, in the normal direction. Then, a strategy can be the use of the *cohesive interaction prope*rty. Cohesive elements are useful in modeling adhesives, bonded interfaces, gaskets, and rock fractures. The cohesive zone is generally discretized with a single layer of cohesive elements through the thick-ness connected to the principal elements. When the cohesive zone represents an infinitesimally thin layer of adhesive at a bonded interface (like it can be assumed for the composite slabs), it may be more relevant to define the response of the interface directly in terms of the traction at the interface versus the relative motion across the interface. In this case the surface-based cohesive behavior option provides a simplified way to model cohesive connections with negligibly small interface thicknesses using the traction-separation constitutive model. The cohesive surface behavior can be defined for general contact in Abaqus/Explicit. Cohesive surface behavior is defined as a surface interaction property. The stiffness coefficient along the principal directions must be defined; following the notation inside the software the normal stiffness, K_{nn}, is set equal to the concrete elastic modulus E_c, while the tangential stiffness, K_{tt} and K_{ss} are equal to the tangential modulus of the concrete G_c. The damage properties are related to the stresses acting on the interface: Normal stress is set equal to the maximum tensile strength of the concrete while the shear stresses are equal to the maximum longitudinal shear strength evaluated by means Eurocode 4 [7]. The evaluation of the shear strength must be always based on experimental findings, following the *design-by-testing* principles [12]

Finally, as previously discussed, to simulate the M-tests the slabs can be considered as partially cracked along their length. For this reason, the numerical models were divided into three different zones (Figure 10): two uncracked zones close to the supports, with an extension equal to L_u, and a central cracked zone, with an extension of L_{cr}. In the central zone the tensile resistance and shear strength was reduced approximately ten times to simulate the crack initiation.

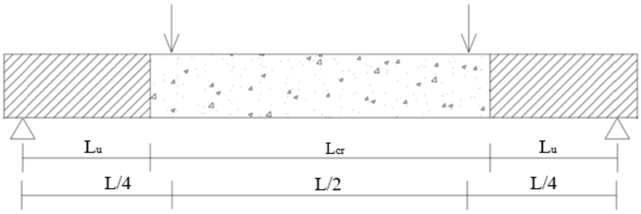

Figure 10: Cracked and uncracked division of the slab.

An example of the results obtained from the numerical modelling phase is reported in Figure 11, for the slab tested in the monotonic test type with 2400 mm of total length. It can be noted that a good approximation of the curve is obtained, in terms of both stiffness and debonding load. Also, the post-slippage stiffness, m_{II}, showed more than good agreement. On the contrary, the loss of stiffness experimentally observed in the last phase of the loading phase, is not completely captured by the model. The interface modelling could be improved. The proposed curve is representative of all the cases.

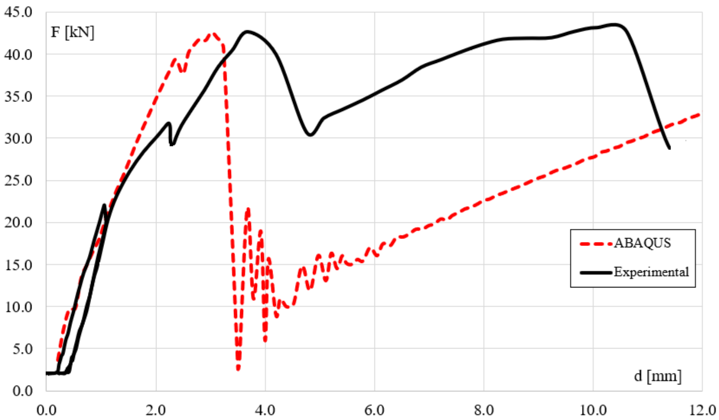

Figure 11: Numerical model results, force-displacement curve for 2400mm slab, Monotonic load.

In table 2 the maximum loads obtained by means of the proposed numerical models are compared with the ones experimentally observed.

Table 2: Experimental vs. numerical debonding load.

Length [mm]	type of test	F_{max_exp} [kN]	F_{max_num} [kN]	exp/num
2000	M	44.3	48.7	0.91
2400	M	42.6	42.5	1.00
2800	M	50.4	54.5	0.93
3200	M	58.6	65.5	0.89
3600	M	66.2	72.8	0.90

In terms of debonding load the maximum difference between the numerical and the experimental value is around 10%. To replicate also the debonding loads of the cyclic tests it is necessary to tune the value of the shear strength without modifying any other parameter. For the design the shear strength to be considered is the one obtained from the C-tests.

5 CONCLUSIONS

The proposed paper investigates the problem of the evaluation of the deformability of composite steel-concrete slabs. In particular, different slabs are characterized by the same materials and cross-section, but different total lengths have been presented. Five different lengths were considered (2000, 2400, 2800, 3200 and 3600 mm) and for each length monotonic and cyclic test protocol were executed. The findings of the paper can be summarized in:

- There is a lack of information for what concerns the correct estimation of the slab deformability. While the resistance has been largely investigated, the deformability has not been deeply resolved.
- the deformability of the slabs is influenced by the distribution of the cracks along the slab length and the level of interaction between the two materials. For the short-term response it is possible to use as flexural stiffness of the total slab the median value between cracked and un-cracked concrete cross-section. On the contrary, when the long-term response is considered, only the cracked response is close to the experimental results;
- the discussed numerical model based on the Cohesive interaction between the steel and the concrete give a good approximation of the debonding load. However, regarding the global deformability it should be refined, especially in the second stage of the deformation, when the slope of the curve decreases.

REFERENCES

[1] R. Abdullah, A.B.H. Kueh, I.S. Ibrahim, W.S. Easterling, Characterization of shear bond stress for design of composite slabs using an improved partial shear connection method, *Journal of Civil Management*, **21(6)**, 720-732, 2015.

[2] V. Bilek, S. Bonczková, J. Hurta, D. Pytlík, M. Mrovec, Bond strength between reinforcing steel and different types of concrete, *Procedia Eng.*, **190**, 243-247, 2017.

[3] C. Bernuzzi, M.A. Pisani, M. Simoncelli, Debonding strain for steel-concrete composite slabs with trapezoidal metal deck. Steel and Composite Structures, **49 (1)**, 19-30, 2023.

[4] M. Crisinel, F. Marimon, A new simplified method for the design of composite slabs, *Journal of Construct. Steel Res.*, **60**, 3-5, 481-491, 2004.

[5] N.A. Hedaoo, L.M. Gupta, G.N. Ronghe, Design of composite slabs with profiled steel decking: a comparison between experimental and analytical studies, *Journal Adv. Struct. Eng.*, **3**, 1-15, 2012.

[6] AS/NZS 2327 Australian/New Zealand standard, Composite Steel-Concrete Construction in Buildings. Sydney/Wellington, 2017.

[7] CEN EN1994-1-1, Eurocode 4: Design of Composite Steel and Concrete Structures – Part 1-1-: General Rules and Rules for Buildings, 2004.

[8] M. Patrick, R.Q. Bridge, Review of Concepts Concerning Bond of Steel Decking. Proc. 12th Int. Spec. Conf. Cold-Form. Steel Struct., Rolla, MO 65409, Stati Uniti: Missouri University of Science and Technology, p. 27, 1999.

[9] G. Ranzi, G. Leoni, R. Zandonini, State of the art on the time-dependent behaviour of composite steel–concrete structures, *J. Construct. Steel Res.*, **80**, 252-263, 2013.

[10] R.S. Costa, A.C.C. Lavall, E.L. Andrade, New equations to establish the effective moment of inertia of composite slabs with profiles steel sheeting for deflection calculation, *J. Build. Eng.*, **37**, 102135, 2021.

[11] Abaqus Finite element software, academic license, Politecnico di Milano, https://www.3ds.com/it/ 2025.

[12] N. Baldassino, C. Bernuzzi, M. Simoncelli, Experimental vs. theoretical design approaches for thinwalled cold-formed steel beam-columns, *Adv. Steel Construct.*, **15(1)**, 55-65, 2019.